OFC 2021 © OSA 2021

Experimental Evaluation of Optical Cross-Connects with Flexible Waveband Routing Function for SDM Networks

Takuma Kuno¹, Yojiro Mori¹, Suresh Subramaniam², Masahiko Jinno³, Hiroshi Hasegawa¹

¹Nagoya University, Furo-cho, Chikusa-ku, Nagoya, 464-8603 Japan ²George Washington University, 800, 22nd St. NW, Washington DC, 20052 USA ³Kagawa University, Hayashi-cho, Takamatsu, Kagawa 761-0396 Japan kuno.takuma@j.mbox.nagoya-u.ac.jp

Abstract: We experimentally evaluate the transmission performance of OXC structures based on flexible-waveband routing. 1600 km, 700 km, and 600 km transmission is demonstrated using 32 Gbaud DP-QPSK, DP-8QAM, and DP-16QAM on 37.5 GHz grid, respectively. © 2021 The Author(s)

1. Introduction

In photonic networks, optical cross-connects (OXCs) can handle wavelength-division multiplexing (WDM) signals without costly optical-to-electrical and electrical-to-optical conversion [1]. Now that capacity of a single-core fiber (SCF) is approaching full utilization, space-division multiplexing (SDM) using multi-core fibers (MCFs) is taken to be an attractive candidate to expand fiber capacity [2-6]. This motivates us to develop an OXC architecture suitable for MCF-based networks while retaining high routing flexibility. The presently deployed OXC for SCF-based networks consists of multiple wavelength-selective switches (WSSs) connected in a broadcast-and-select or route-and-select manner [1]. This OXC architecture fails to suit port-hungry SDM networks because the number of costly WSSs increases super-linearly with the OXC port count [7]. The use of joint-switch WSSs (JS-WSSs) can reduce the hardware cost [8]; however, this approach yields low routing flexibility in that the channels with the same wavelength in an incoming MCF must be delivered to the same outgoing MCF. Another candidate, the core-wise switching OXC architecture, can attain almost the same routing flexibility as the non-restricted OXC [9]; however, many WSSs are required.

Given this background, we previously proposed an OXC architecture based on spatially jointed flexible-waveband routing [10]. In the proposed architecture, delivery-and-coupling (DC) space switches that consist of optical selectors and optical couplers are inserted between JS-WSSs for relaxing the JS-WSS routing restriction. The routing flexibility is attained in return for the additional loss created by the DC space switch. Network simulations have already shown that the OXC based on flexible-waveband routing has almost the same routing performance as the non-restricted OXC while suppressing the hardware cost [10,11]. Furthermore, a proof-of-concept experiment showed the feasibility of the OXC architecture [11]; 700 km transmission and 7-node traversal of 400 Gbps DP-16QAM signals was successfully demonstrated under a particular condition.

This paper considers more system parameters and clarifies the applicable network scale of the OXC architecture with flexible-waveband routing. The modulation order and DC space switch scale are used as parameters. Through transmission experiments on 32 Gbaud DP-4QAM, DP-8QAM, and DP-16QAM signals aligned on a 37.5 GHz grid, transmission distances of 1600 km, 700 km, and 600 km are demonstrated, respectively. Such results show that our OXC architecture is applicable to most metro-scale networks. The results of the experiment will benefit the design of OXCs and networks based on SDM.

2. OXC architecture based on flexible-waveband routing

Figure 1 shows the OXC architecture based on flexible-waveband routing [11]. Here, n incoming M-core fibers are virtually bundled. Thus, nN incoming M-core fibers and nN outgoing M-core fibers are used for making an $nNM \times nNM$ OXC, where the OXC port count is nNM in terms of the number of cores. The $nNM \times nNM$ OXC comprises nN M-array $1 \times B$ JS-WSSs, nMB $N \times N$ DC space switches, and nN M-array $B \times 1$ JS-WSSs. Note that $N \times N$ DC space switch can be fabricated cost-effectively as planer-lightwave circuits or silicon photonics technology [12,13]. The routing operation is composed of three processes: First, optical paths from incoming MCFs are grouped into B flexible wavebands by n M-array of $1 \times B$ JS-WSSs. Note that the frequency demarcations of wavebands match those among the MCFs in the same bundle. Next, the B flexible wavebands are independently routed to the JS-WSS connected to the outgoing MCF by an $N \times N$ DC space switch. Finally, multiple flexible wavebands are coupled by $B \times 1$ JS-WSSs. By combining JS-WSSs and DC space switches, a flexible waveband can be delivered to more outgoing fibers.

The maximum number of accessible adjacent nodes is *BN*, *i.e.* the product of JS-WSS degree and DC space switch degree. In other words, routing flexibility is improved by increasing *B* or *N*. However, increasing *B* is infeasible because the total number of the input and output ports of feasible JS-WSSs is limited to around 35+. Expanding the DC space switch degree is cost-effective; however, the insertion loss due to optical couplers in the DC space switch increases with *N*. Therefore, *N* must be determined considering the network scale and transmission performance.

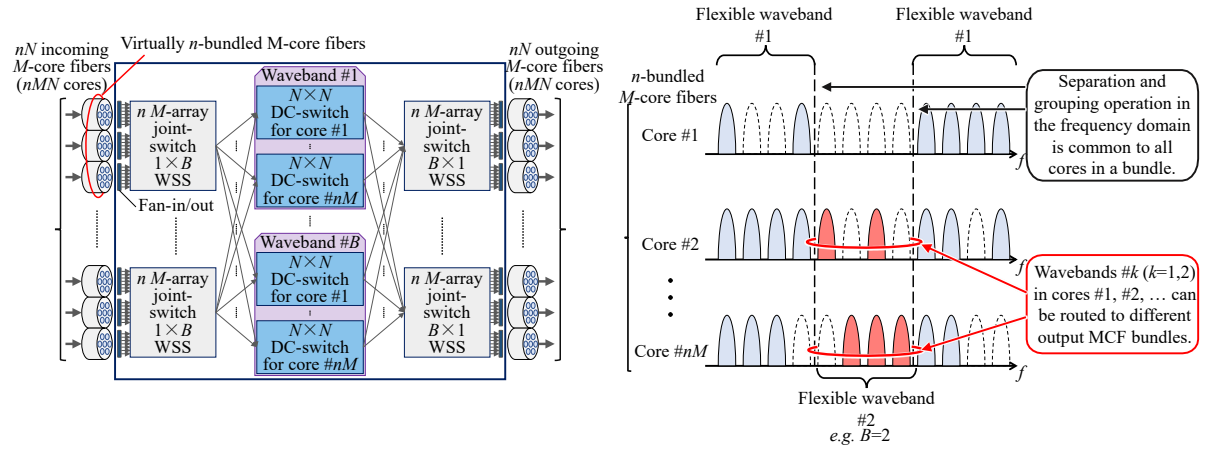


Fig.1. The OXC architecture based on flexible-waveband routing

3. Experiments

We conducted transmission experiments to evaluate the performance of our OXC architecture. Due to the limited device availability, we used SCFs for the transmission links; note that similar results can be expected for MCF-based systems because OXC devices placed between fan-in/outs are fabricated for SCFs. Figure 2 shows the experimental setup. At the transmitter side, a continuous wave (CW) was generated by a tunable laser. A 32 Gbaud 4QAM/8QAM/16QAM signal was created by a lithium-niobate IQ modulator (IQM) driven by an arbitrary-waveform generator (AWG). Next, the dual-polarization signal was created by a polarization-division multiplexing (PDM) emulator comprised of polarization-beam splitter (PBS), a 10-ns-delay fiber, and polarization-beam coupler (PBC). As non-target signals, we created 64-wavelength 32 Gbaud DP-QAM signals by using a 64-CW source, an IQM, and a PDM emulator. A gain-flattening filter (GFF) was used to flatten the WDM signal power and remove the signal that occupies the frequency slot of the target signal. The target signal and non-target signals were combined at a 2×1 coupler yielding 64-channel 32 Gbaud DP-QAM signals aligned on a 37.5 GHz grid. The signal launch power was adjusted by an erbium-doped fiber amplifier (EDFA) and a variable optical attenuator (VOA). The signals entered a link-and-OXC loop consisting of two synthesized loop-controlling switches (SWs), a 2×2 splitter, a 100 km SCF, an EDFA, the OXC under test, an EDFA, and a VOA. The OXC consisted of 7-array 1×2 JS-WSS, N×N DC space switch part, and 7-array 2×1 JS-WSS. The $N\times N$ DC space switch part was emulated by combining $1\times N$ optical selector and VOA. In the OXC, the target signal and the other non-target signals were decorrelated in a route-delay-select manner using JS-WSS, delay fiber, and JS-WSS. The loss coefficient, nonlinearity coefficient, and dispersion parameter of the SCF were 0.18 dB/km, 1.5/W/km, and 16.5 ps/nm/km, respectively. The noise figure of EDFA was around 5 dB. The output power of the EDFA ahead of the OXC was set to 9 dBm per wavelength; note that the EDFA power is set to such a high power to evaluate a large measurement range. The loss of each JS-WSS is 10 dB. The loss of the DC space switch is parameterized. Note that the SNR determiner regarding OXC is the signal power per wavelength after OXC traversal, P_{out} . After loop circulation, the signals entered a 100 km SCF. Finally, the target signal was extracted by an optical tunable filter (TF) and detected by a digital coherent receiver. The digital signal processing circuit executed polarization recovery, carrier-phase estimation, frequency estimation, receiver-side IQ related impairments compensation, and symbol decoding.

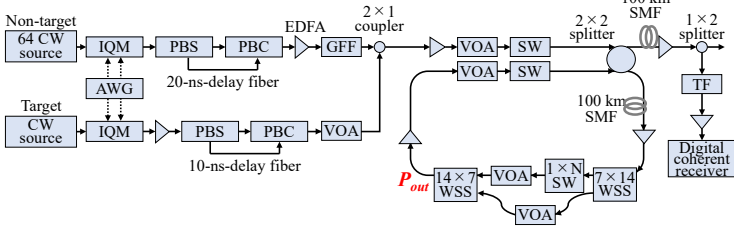


Fig. 2. The experimental setup.

Th4E.3 OFC 2021 © OSA 2021

Figure 3 plots the BERs versus hop count, where the acceptable BER threshold was set to 2.7×10^{-2} assuming the use of forward error correction [14]. When $P_{\text{out}} = -21$ dBm, 4QAM, 8QAM, and 16QAM signals can be transmitted over 16, 7, and 6 node hops, respectively. The corresponding transmission distance are 1600 km, 700 km, and 600 km. These results indicate that our proposed OXC can cover most metro networks even though its hardware cost is much lower than those of conventional OXCs.

Figure 4 shows the attainable port count of a DC space switch, where the transmissible distance L and signal power per wavelength after the OXC P_{out} are parametrized. The loss of $N \times N$ DC space switch is defined as $10\log_{10}N + 1$ dB including excess loss. When $P_{\text{out}} = -21$, OXC-input power per wavelength and DC-switch loss including excess loss correspond to 6 dBm and 7 dB, respectively. Regardless of modulation format, the port count of the DC space switch can be at least 4×4 if 6 dB intrinsic loss and 1 dB excess loss are considered; the literature shows that the use of 4×4 DC space switches can offer sufficient routing flexibility in most network topologies [11]. Thus, we confirmed that our OXC architecture offers enough transmission performance and routing flexibility for use in metro networks.

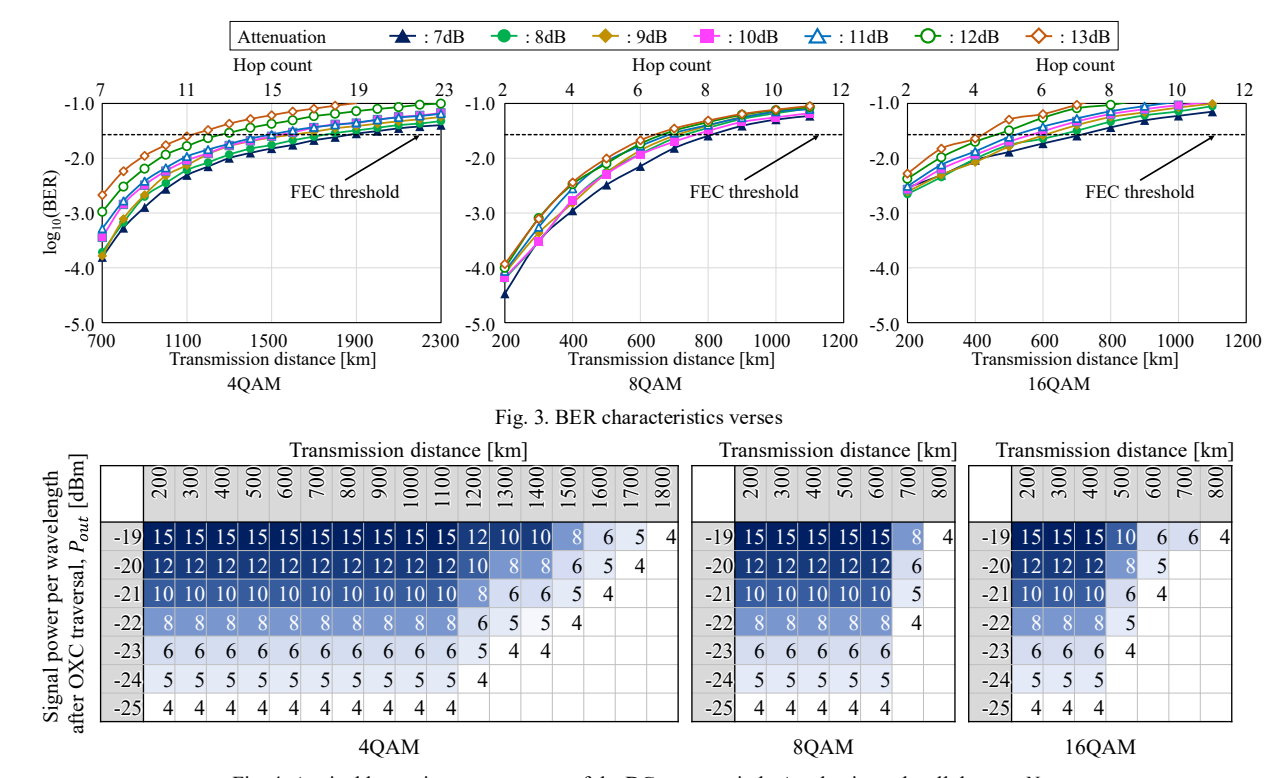


Fig. 4. Attainable maximum port count of the DC space switch. A value in each cell denotes N.

5. Conclusion

We evaluated the feasibility of our proposed OXC architecture and clarified the relation between applicable network scale and OXC requirements. Experiments showed that the proposed OXC with its sufficient routing flexibility and transmission performance well suits metro networks. The results will allow the OXCs suitable for given networks to be designed. Our cost-effective OXC architecture will overcome the barriers to the realization of SDM networks.

Acknowledgements: This work was supported in part by NICT and NSF.

6. References

- [1] S. L. Woodward et al., Optical Fiber Telecommunications Volume VIB Sixth Edition: Systems and Networks, Academic Press (2013).
- [2] D. J. Richardson et al., Nat. Photonics 7, 354-362 (2013).
- [3] G. Li et al., OSA Adv. Opt. Photonics 6, 413-487 (2014).
- [4] G. M. Saridis *et al.*, IEEE Commun. Surv. Tut. **17**, 2136-2156 (2015)
- [5] P. J. Winzer, Opt. Photonics News 26, 28-35 (2015).
- [6] D. Soma et al., IEEE/OSA J. Lightw. Technol. 36, 1362-1368 (2018).
- [7] M. Niwa et al., IEEE/OSA J. Opt. Commun. Netw. 9, A1-A25 (2017).
- [8] L. E. Nelson *et al.*, IEEE/OSA J. Lightw. Technol. **32**, 783-789 (2013).
- [9] F.-J. Moreno-Muro *et al.*, IEEE/OSA J. Opt. Commun. Netw. 9, 1041-1050 (2017).
- [10] H. Hasegawa *et al.*, ECOC, Th.1.A.P63 (2019).
- [11] T. Kuno et al., ONDM, S6.4 (2020).
- [12] T. Watanabe *et al.*, OFC, OTh3D.1 (2012).
- [13] S. Nakamura *et al.*, IEEE J. Sel. Top. Quantum Electron. 22, 185-193 (2016).
- [14] D. Chang et al., OFC, OW1H.4 (2012).